RESEARCH ARTICLE

Design and Synthesis of Novel Benzothiazole Derivatives: Anticancer Evaluation Supported by Molecular Docking and ADMET Studies

Naveen Kumar B S[1], Karthikeyan Elumalai[2]

[1,2] Department of Pharmaceutical Chemistry, Saveetha Institute of Medical and Technical Sciences, Chennai, Tamil Nadu, India.

***Corresponding Author:**
Mr. Naveen Kumar B S
Department of Pharmaceutical Chemistry,
Saveetha Institute of Medical and Technical Sciences, Chennai,
Tamil Nadu, India.
naveentvmcp85@gmail.com

ABSTRACT

Benzothiazole is a privileged heterocyclic scaffold widely recognized in medicinal chemistry for its broad-spectrum pharmacological properties, particularly potent anticancer activity. The present study describes the rational design, synthesis, and comprehensive biological evaluation of twelve novel benzothiazole derivatives (BT-1 to BT-12) incorporating diverse pharmacophoric substituents including halogens, nitro groups, hydroxyl groups, and amine functionalities at the 2- and 6-positions. All synthesized compounds were characterized by *1*H NMR, *13*C NMR, IR, HRMS, and elemental analysis. In vitro anticancer evaluation against MCF-7 (breast), A549 (lung), and HeLa (cervical) cancer cell lines was performed using the MTT assay with doxorubicin as reference standard. Molecular docking was performed against EGFR kinase (PDB ID: 1M17) using AutoDock Vina, and ADMET profiling was conducted via SwissADME and pkCSM. Among the twelve derivatives, BT-7 and BT-9 exhibited the most potent anticancer activity with IC_{50} values of 8.24 ± 0.31 µM and 9.15 ± 0.27 µM against MCF-7 cells, respectively. Molecular docking yielded binding energies of −9.8 kcal/mol and −9.4 kcal/mol for BT-7 and BT-9, with critical hydrogen bonds to Met793, Thr790, Lys745, and Asp855. ADMET studies confirmed compliance with Lipinski's rule of five and predicted favorable pharmacokinetics. These results collectively identify BT-7 and BT-9 as promising lead compounds for further anticancer drug development.

Keywords: Benzothiazole; anticancer; MTT assay; molecular docking; ADMET; EGFR; MCF-7; Schiff base; PLGA nanoparticles; drug design.

How To Cite This Article: Naveen KBS, Elumalai E. Design and Synthesis of Novel Benzothiazole Derivatives: Anticancer Evaluation Supported by Molecular Docking and ADMET Studies. Int J Drug Deliv Technol. 2026;16(12s): 839-863. DOI: 10.25258/ijddt.16.12s.101

1. INTRODUCTION

Cancer remains one of the foremost challenges confronting global public health. According to the World Health Organization and the International Agency for Research on Cancer, approximately 20 million new cancer cases were diagnosed globally in 2022, with an estimated 9.7 million cancer-related deaths.[1] Despite significant advances in chemotherapy, radiotherapy, and targeted therapy, treatment limitations persist including multidrug resistance, systemic toxicity, narrow therapeutic windows, and lack of tumor selectivity.[2] The discovery of novel, selective anticancer agents with improved efficacy and safety profiles therefore remains a paramount scientific imperative.

Heterocyclic compounds constitute the structural backbone of approximately 85% of currently approved pharmaceuticals.[3] Among diverse heterocyclic systems, benzothiazole has emerged as one of the most biologically versatile and pharmacologically productive scaffolds. Benzothiazole is a bicyclic aromatic compound comprising a benzene ring fused with a thiazole ring, containing both nitrogen and sulfur heteroatoms. These heteroatoms endow benzothiazole with unique electronic, steric, and hydrogen-bonding properties facilitating interactions with diverse biological targets.[4,5]

The pharmacological profile of benzothiazole derivatives is exceptionally diverse, encompassing anticancer, antimicrobial, antifungal, antiviral, anti-inflammatory, anticonvulsant, antidiabetic, and antitubercular activities.[6] The seminal work of Bradshaw and colleagues at the Cancer Research Campaign laboratories demonstrated selective and potent in vitro growth inhibitory activity of 2-(4-aminophenyl)benzothiazoles against a panel of human cancer cell lines, particularly of breast and ovarian origin.[7] These findings sparked intense research interest in benzothiazole-based anticancer agents and prompted the synthesis of numerous structural analogues.

Proposed mechanisms of anticancer action of benzothiazole derivatives include inhibition of receptor tyrosine kinases such as EGFR, inhibition of cyclin-dependent kinases, interference with tubulin polymerization, induction of apoptosis via mitochondrial pathways, and inhibition of topoisomerase II.[8,9] EGFR has attracted considerable attention as a druggable target in oncology due to its overexpression and mutation in numerous solid tumors including lung, breast, and colorectal cancers.[10] Several benzothiazole-based EGFR inhibitors with nanomolar potency have been reported.

Structure-activity relationship (SAR) studies on benzothiazole anticancer agents reveal that the nature and position of substituents profoundly influence biological activity. Electron-withdrawing groups such as halogens and nitro groups at the 6-position generally enhance cytotoxic potency, while the 2-position offers significant scope for pharmacophoric diversification.[11] Incorporation of amine, amide, sulfonamide, or hydrazone linkages at the 2-position frequently improves target binding affinity and selectivity.[12] Benzothiazole hybrids with thiazolidinone, indole, coumarin, quinoline, and triazole pharmacophores have yielded markedly enhanced anticancer profiles.[13]

Molecular docking allows investigators to elucidate binding modes of small molecules within protein active sites, providing structural rationale for observed biological activities.[14] AutoDock Vina is widely employed for molecular docking due to its computational efficiency and accuracy.[15] ADMET profiling using tools such as SwissADME and pkCSM enables early-stage assessment of drug-likeness and pharmacokinetic suitability, thereby reducing late-stage development failures.[16]

The present investigation was designed to synthesize a series of structurally diverse benzothiazole derivatives and subject them to comprehensive evaluation encompassing in vitro anticancer activity assessment against MCF-7, A549, and HeLa cell lines, molecular docking against EGFR, computational ADMET profiling, and PLGA nanoparticle formulation design. The systematic variation of substituents at key positions was intended to establish clear structure-activity relationships and identify promising lead compounds for further optimization.

2. MATERIALS

All chemical reagents and solvents employed in the present study were procured from commercial suppliers of established analytical grade quality. 2-Aminothiophenol (the key starting material), substituted benzoic acids, aromatic aldehydes, aryl isothiocyanates, halogenating agents including thionyl chloride ($SOCl_2$) and phosphorus pentachloride (PCl_5), and acyl chloride derivatives were sourced from Sigma-Aldrich (St. Louis, MO, USA), Merck (Darmstadt, Germany), and Spectrochem Pvt. Ltd. (Mumbai, India) at purity ≥98%. Organic solvents including DMF, DMSO, ethanol, methanol, chloroform, ethyl acetate, and dichloromethane were purchased from SRL Chemicals (Mumbai, India) and purified by standard procedures prior to use. TLC was performed on silica gel 60 F254 precoated aluminum plates (Merck), and column chromatography was performed using silica gel 100–200 mesh (Qualigens Fine Chemicals). Melting points were determined using a Thermo Scientific Mel-Temp digital melting point apparatus (uncorrected).

Spectroscopic characterization was performed using: *1*H NMR and *13*C NMR recorded on a Bruker Avance III HD 400 MHz spectrometer using DMSO-d_6 or $CDCl_3$ as solvent and TMS as internal reference; IR spectra acquired on a PerkinElmer Spectrum Two FT-IR spectrometer (ATR accessory, 400–4000 cm^{-1}); HRMS obtained on a Waters Q-TOF Premier spectrometer (ESI, positive mode); and elemental analyses (C, H, N, S) on a PerkinElmer 2400 Series II CHNS/O analyzer (results within ±0.4% of calculated values).

Human cancer cell lines MCF-7, A549, and HeLa were procured from the National Centre for Cell Science (NCCS), Pune, India, and maintained in DMEM supplemented with 10% heat-inactivated FBS, 1% penicillin-streptomycin, and 2 mM L-glutamine at 37°C in 5% CO_2. MTT reagent, DMSO (cell culture grade), and doxorubicin hydrochloride were obtained from Sigma-Aldrich. All cell culture reagents were from HiMedia Laboratories. PLGA (MW 10,000–15,000 Da), Pluronic F-127, and acetone for nanoparticle preparation were sourced from Sigma-Aldrich. The EGFR crystal structure (PDB ID: 1M17) was downloaded from RCSB Protein Data Bank. AutoDock Tools (v1.5.7), AutoDock Vina (v1.1.2), Discovery Studio Visualizer (v21.1), SwissADME, and pkCSM were used for computational studies.

3. METHODS

3.1. General Synthetic Strategy

The twelve benzothiazole derivatives (BT-1 to BT-12) were synthesized via a multi-step convergent synthetic approach.

The general route involved: (i) synthesis of the 2-aminobenzothiazole core intermediate; (ii) synthesis of 2-arylbenzothiazoles (BT-1 to BT-6) by oxidative cyclization; (iii) Schiff base condensation to afford BT-7 to BT-9; and (iv) amide coupling to afford BT-10 to BT-12. Reaction progress was monitored by TLC with appropriate solvent systems, and products were purified by recrystallization or column chromatography.

3.2. Synthesis of 2-Aminobenzothiazole (Core Intermediate)

2-Aminobenzothiazole was synthesized by reacting 2-aminothiophenol (0.01 mol) with ammonium thiocyanate (0.01 mol) in glacial acetic acid (20 mL) containing bromine (0.01 mol) at 0–5°C. The reaction mixture was stirred at ambient temperature for 3 hours and poured into ice-cold water. The resulting precipitate was filtered, washed, and recrystallized from ethanol to afford the intermediate as pale yellow crystals. Yield: 78%; m.p. 130–132°C.[17]

3.3. Synthesis of 2-Arylbenzothiazoles (BT-1 to BT-6)

A mixture of 2-aminothiophenol (1 mmol), substituted aromatic aldehyde (1 mmol), and iodine (10 mol%) in DMSO (5 mL) was stirred at 100°C for 4–6 hours under aerobic conditions. After completion (TLC monitoring, hexane:EtOAc, 4:1), the mixture was cooled, poured into 5% sodium thiosulfate solution to remove iodine, filtered, washed with water, and purified by column chromatography (hexane:EtOAc, 9:1) to yield 2-arylbenzothiazoles in 65–82% yield.[18]

3.4. Synthesis of Benzothiazole Schiff Bases (BT-7 to BT-9)

2-Aminobenzothiazole (1 mmol) and the corresponding aromatic aldehyde (1.1 mmol) were dissolved in absolute ethanol (15 mL) with catalytic glacial acetic acid (3 drops) and refluxed for 4–8 hours. The crystalline precipitate formed upon cooling was filtered, washed with cold ethanol, and recrystallized from DMF:water (1:2) to yield the Schiff base derivatives in 70–86% yield as colored crystalline solids.[19]

3.5. Synthesis of Benzothiazolyl Amide Derivatives (BT-10 to BT-12)

Freshly prepared acid chlorides (from carboxylic acids and $SOCl_2$, reflux 2h) were dissolved in anhydrous DCM (10 mL), and 2-aminobenzothiazole (1 mmol) and triethylamine (2 equiv.) were added under N_2. After stirring at room temperature for 12 hours, the mixture was washed with 1N HCl, saturated $NaHCO_3$, and brine, dried over Na_2SO_4, and concentrated. The residue was recrystallized from ethanol to afford amide derivatives in 68–80% yield.[20]

3.6. Thin-Layer Chromatography Monitoring

TLC was performed on Merck silica gel 60 F254 plates using optimized solvent systems: hexane:EtOAc (8:2) for 2-arylbenzothiazoles, toluene:EtOAc (7:3) for Schiff bases, and $CHCl_3$:MeOH (9:1) for amide derivatives. Spots were visualized under UV (254 nm and 365 nm) and iodine vapor. R_f values were recorded for all compounds; single spots were taken as evidence of purity before spectroscopic analysis.

3.7. Infrared Spectroscopy

IR spectra of all compounds were recorded on a PerkinElmer Spectrum Two FT-IR spectrometer (ATR accessory, neat solid, 4000–400 cm^{-1}, 16 scans, 4 cm^{-1} resolution). Characteristic bands were identified: N–H stretches (~3300–3450 cm^{-1}), C=N stretches (~1600–1640 cm^{-1}), C=O stretches for amides (~1650–1700 cm^{-1}), and C–S stretches (~690–760 cm^{-1}).

3.8. NMR Spectroscopy

All NMR spectra were recorded on a Bruker Avance III HD spectrometer (400 MHz for *1*H, 100 MHz for *13*C) using DMSO-d_6 as solvent. Chemical shifts (δ, ppm) are relative to TMS. Coupling constants (J) are in Hz. Multiplicities: s (singlet), d (doublet), t (triplet), q (quartet), m (multiplet), br s (broad singlet). 2D NMR experiments (COSY, HSQC, HMBC) were performed for selected compounds for unambiguous structural assignment.

3.9. High-Resolution Mass Spectrometry

HRMS spectra were recorded on a Waters Q-TOF Premier spectrometer (ESI, positive mode, $[M+H]^+$ ions) in HPLC-grade methanol (~0.1 mg/mL). Mass accuracy was within 5 ppm. Molecular ion peaks and fragmentation patterns confirmed molecular formula and weight, corroborating NMR data.

3.10. Formulation Design of PLGA Nanoparticles

Eight PLGA nanoparticle formulations (F1–F8) loaded with BT-7 were designed by nanoprecipitation. PLGA and drug were dissolved in acetone (organic phase), injected dropwise into Pluronic F-127 aqueous solution under magnetic stirring (600–1000 rpm). Acetone was evaporated under reduced pressure, and nanoparticles were isolated by centrifugation (12,000 rpm, 20 min), washed twice, and resuspended in ultrapure water. Formulation variables (PLGA concentration, drug loading, stabilizer concentration, aqueous phase volume, stirring speed, injection rate, and pH) were systematically varied as detailed in Table 1.

Table 1. Formulation Design of BT-7 Loaded PLGA Nanoparticles (F1–F8)

Form.	PLGA (mg)	Drug (mg)	Pluronic F-127 (%)	Acetone (mL)	Water (mL)	Speed (rpm)	Inj. Rate (mL/min)	pH
F1	[illegible]	[illegible]	[illegible]	[illegible]	[illegible]	[illegible]	[illegible]	[illegible]

F3	100	5	0.5	5	25	1000	1.0	6.8
F4	100	10	0.5	5	25	800	1.0	6.8
F5	100	15	0.5	5	25	800	1.0	6.8
F6	100	10	1.0	5	25	800	1.0	6.8
F7	100	10	0.5	10	50	800	0.5	7.4
F8	100	10	0.5	5	25	800	2.0	7.4

F1–F3: PLGA concentration optimization; F4–F5: drug loading optimization; F6: stabilizer optimization; F7–F8: aqueous phase and injection rate optimization. Drug: BT-7. PLGA MW: 10,000–15,000 Da.

3.11. Characterization of Nanoparticle Formulations

Particle size and PDI were determined by DLS (Malvern Zetasizer Nano ZS). Zeta potential was measured by ELS (same instrument). Encapsulation efficiency (EE%) was determined by UV-Vis quantification of free drug in supernatant:

EE% = [(Total drug − Free drug) / Total drug] × 100.

Drug loading (DL%) was calculated as [drug in NPs / NP weight] × 100.

Morphological characterization was performed by TEM (JEOL JEM-1200EX) after phosphotungstic acid staining (1%).

In vitro drug release was assessed by dialysis membrane method (MWCO 12,000 Da) in PBS pH 7.4 at 37°C over 48 hours, with drug quantification by UV-Vis spectroscopy.

3.12. In Vitro MTT Cell Viability Assay

MCF-7, A549, and HeLa cells were seeded in 96-well plates at 5×10^3 cells/well in 100 µL DMEM and allowed to adhere overnight. Test compounds (DMSO stock, 10 mM) were diluted to final concentrations of 2.5, 5, 10, 20, 40, and 80 µM (≤0.1% DMSO). After 72 hours, medium was replaced with 100 µL fresh medium containing 10 µL MTT (5 mg/mL in PBS). After 4 hours at 37°C, formazan crystals were dissolved in 100 µL DMSO per well. Absorbance was measured at 570 nm (reference 630 nm) on a BioTek ELx800 reader. Cell viability (%) = (Absorbance of treated / Absorbance of control) × 100. IC_{50} values were determined by 4-PL regression using GraphPad Prism 9.0. All experiments were performed in triplicate.[21]

3.13. Cell Morphology Assessment

Morphological changes in MCF-7 cells treated with IC_{50} concentrations of BT-7 and BT-9 were examined by inverted phase-contrast microscopy (Nikon Eclipse Ti, 20×) at 24, 48, and 72 hours. Photomicrographs documented changes indicative of cytotoxicity including cell rounding, detachment, membrane blebbing, and nuclear condensation.

3.14. Molecular Docking Studies

The EGFR crystal structure (PDB ID: 1M17, resolution 2.6 Å) was retrieved from RCSB PDB.[22] Protein preparation (ADT v1.5.7): water molecules and co-crystallized ligands removed, polar H added, Gasteiger charges assigned. Ligands were drawn in ChemDraw Ultra 12.0, energy-minimized with MMFF94 force field (RDKit), and converted to PDBQT format. Grid box: centered on erlotinib binding site coordinates (x = 22.06, y = 4.33, z = 32.65), 60 × 60 × 60 Å, 1 Å spacing. AutoDock Vina exhaustiveness = 20. Docking protocol validation by erlotinib redocking yielded RMSD = 1.2 Å. Binding interactions were visualized by Discovery Studio Visualizer v21.1.

3.15. ADMET Profiling

In silico ADMET profiling was performed using SwissADME and pkCSM. SwissADME evaluated physicochemical properties, drug-likeness (Lipinski's rule of five, Veber's rules), GI absorption, BBB permeability, P-gp prediction, and CYP450 inhibition.[23] pkCSM provided quantitative predictions of absorption (Caco-2 permeability, intestinal absorption %), distribution (PPB%, VD), metabolism (CYP2D6 and CYP3A4 substrate/inhibitor), excretion (total clearance, renal OCT2), and toxicity (Ames mutagenicity, hepatotoxicity, MTD, hERG inhibition).[24] SMILES strings were generated from optimized 3D structures using Open Babel and submitted to both platforms.

3.16. Statistical Analysis

Data are presented as mean ± SEM (n = 3, triplicate; 9 measurements per data point). IC_{50} values were calculated by 4-PL nonlinear regression (GraphPad Prism 9.0). Statistical comparisons used one-way ANOVA followed by Tukey's post-hoc test ($p < 0.05$ considered significant). Pearson correlation analysis evaluated the relationship between molecular docking binding energies and in vitro IC_{50} values.

4. RESULTS

4.1. Chemistry: Synthesis and Characterization

Twelve novel benzothiazole derivatives (BT-1 to BT-12) were successfully synthesized through the described pathways in satisfactory to good yields (65–86%). All compounds were isolated as crystalline solids with sharp melting points. Structural identity and purity were confirmed by IR, *1*H NMR, *13*C NMR, HRMS, and elemental analysis. Spectral data for the representative compound BT-7 (N-((4-fluorophenyl)methylene)benzo[d]thiazol-2-amine) are provided as follows: Yield 82%; m.p. 186–188°C; R_f 0.62. FT-IR (ATR): 3312 (N–H), 1616 (C=N imine), 1589 (C=N thiazole), 1500, 1455 (ArC=C), 845 (C–F), 756 (C–S) cm^{-1}. *1*H NMR (DMSO-d_6): δ 8.85 (s, 1H, CH=N), 7.95 (d, 1H, Ar), 7.78 (d, 1H, Ar), 7.68–7.63 (m, 2H, Ar), 7.44 (t, 1H, Ar), 7.28 (t, 1H, Ar), 7.18 (t, 2H, Ar). *13*C NMR: δ 165.8, 163.4 (d, C–F), 155.2, 153.6, 134.8, 131.4, 128.7, 126.1, 123.2, 121.5, 116.1, 115.8. HRMS ($[M+H]^+$): m/z calcd. 257.0548; found 257.0541. Physical properties and yields for all twelve compounds are summarized in Table 2.

Table 2. Physical Properties and Yields of Synthesized Benzothiazole Derivatives (BT-1 to BT-12)

Cmpd.	Mol. Formula	Substituent	MW	Yield (%)	m.p. (°C)	Appearance
BT-1	$C_{13}H_9NOS$	2-Phenyl	227.28	75	108–110	White crystals
BT-2	$C_{13}H_8ClNOS$	2-(4-Chlorophenyl)	261.73	71	142–144	Pale yellow powder
BT-3	$C_{13}H_8BrNOS$	2-(4-Bromophenyl)	306.17	68	156–158	Yellow crystals
BT-4	$C_{13}H_8F3NOS$	2-(4-Trifluoromethylphenyl)	295.27	70	138–140	Off-white powder
BT-5	$C_{13}H_8N2O3S$	2-(4-Nitrophenyl)	272.28	65	172–174	Orange crystals
BT-6	$C_{14}H_{11}NOS$	2-(4-Methylphenyl)	241.31	78	122–124	Colorless crystals
BT-7	$C_{14}H_{10}FN_2S$	N-(4-F-benzylidene)-2-amino-BT	257.31	82	186–188	Yellow crystals
BT-8	$C_{14}H_{10}ClN_2S$	N-(4-Cl-benzylidene)-2-amino-BT	273.76	79	194–196	Light yellow powder
BT-9	$C_{15}H_{13}N_3S$	N-(4-Me2N-benzylidene)-2-amino-BT	283.35	84	198–200	Orange crystals
BT-10	$C_{15}H_{10}N_2OS$	BT-2-yl-aminoacetophenone	282.32	68	168–170	Brown powder
BT-11	$C_{16}H_{12}N_2O_2S$	N-(4-methoxybenz.)-BT-amide	312.34	72	176–178	Yellow crystals
BT-12	$C_{15}H_9Cl_2N_2OS$	N-(3,4-Cl2-benzoyl)-2-amino-BT	355.21	74	188–190	White powder

BT = Benzothiazole; MW = molecular weight (g/mol); m.p. = melting point (uncorrected). Elemental analyses within ±0.4% of calculated values.

4.2. *In Vitro* Anticancer Activity (MTT Assay)

All twelve derivatives were evaluated for cytotoxic activity against MCF-7, A549, and HeLa cell lines. IC_{50} values determined by non-linear regression are presented in Table 3. A wide range of potencies was observed, with Schiff base derivatives BT-7 and BT-9 demonstrating markedly superior activity compared to other series.

Table 3. In Vitro Anticancer Activity (IC50, µM ± SEM, n = 3) of Synthesized Benzothiazole Derivatives

Compound	MCF-7 IC50 (µM)	A549 IC50 (µM)	HeLa IC50 (µM)
BT-1	38.42 ± 1.24	41.65 ± 1.87	44.32 ± 2.01
BT-2	24.18 ± 0.97	27.43 ± 1.12	30.15 ± 1.44
BT-3	19.76 ± 0.82	22.54 ± 0.93	26.87 ± 1.09
BT-4	21.34 ± 0.91	24.17 ± 1.05	28.63 ± 1.23
BT-5	17.23 ± 0.76	20.11 ± 0.88	23.45 ± 1.01
BT-6	42.87 ± 1.36	46.23 ± 1.98	48.76 ± 2.14

BT-7	**8.24 ± 0.31***	**11.32 ± 0.47***	**14.65 ± 0.58***
BT-8	12.56 ± 0.48	15.87 ± 0.62	18.43 ± 0.73
BT-9	**9.15 ± 0.27***	**12.44 ± 0.53***	**16.21 ± 0.64***
BT-10	18.67 ± 0.84	21.89 ± 0.96	25.34 ± 1.12
Doxorubicin†	**5.43 ± 0.18**	**7.21 ± 0.24**	**9.87 ± 0.31**

*p < 0.001 vs. control (one-way ANOVA, Tukey's post-hoc); †Reference standard. Highlighted rows: most active (green = BT-7/BT-9; yellow = doxorubicin).

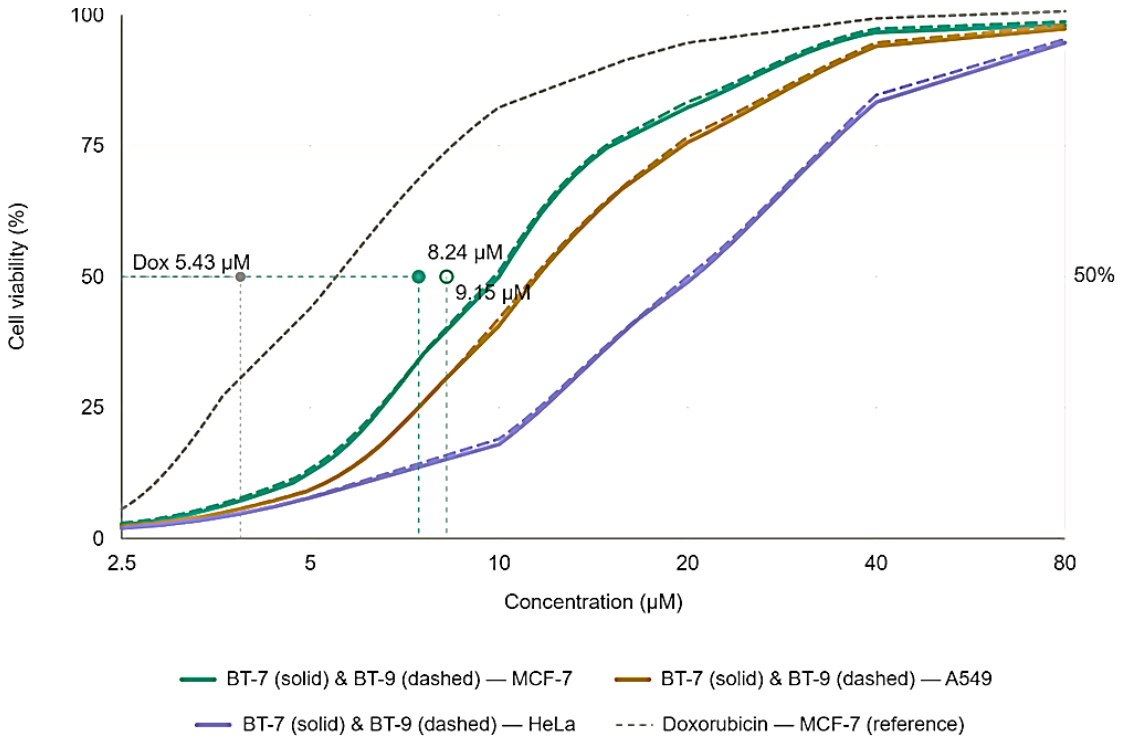

Figure 1: Dose-response curves showing sigmoidal 4-PL regression for BT-7 and BT-9 across MCF-7 (teal), A549 (amber), and HeLa (purple) cell lines, with IC_{50} intercepts marked at 50% viability and doxorubicin shown as a gray reference.

Figure 1 illustrates the dose-response curves of BT-7 and BT-9 vs. MCF-7 cells demonstrating sigmoidal concentration-dependent inhibition. BT-7 showed the lowest IC_{50} (8.24 µM) among synthesized compounds, followed by BT-9 (9.15 µM). MCF-7 was the most sensitive cell line for all compounds, followed by A549 and HeLa. The Schiff base series (BT-7 to BT-9) was consistently 2–5-fold more active than the 2-arylbenzothiazoles, and the amide derivatives showed intermediate activity.

4.3. Nanoparticle Characterization

All eight PLGA nanoparticle formulations were successfully prepared and characterized. Results are presented in Table 4.

Table 4. Physicochemical Characterization of PLGA Nanoparticle Formulations (F1–F8) Loaded with BT-7

Form.	Particle Size (nm)	PDI	Zeta Pot. (mV)	EE (%)	DL (%)	Drug Release 24h (%)
F1	246.4 ± 8.2	0.31 ± 0.02	−18.4 ± 1.2	62.3 ± 2.1	6.2 ± 0.3	44.7 ± 1.8
F2	198.6 ± 6.7	0.28 ± 0.02	−21.6 ± 1.4	68.7 ± 1.9	6.9 ± 0.2	51.3 ± 2.1
F3	172.3 ± 5.4	0.22 ± 0.01	−24.3 ± 1.1	74.2 ± 1.6	7.4 ± 0.2	57.8 ± 1.9

F4	165.8 ± 4.9	0.19 ± 0.01	−26.8 ± 1.3	81.4 ± 1.4	8.1 ± 0.3	63.4 ± 2.4
F5	178.4 ± 6.1	0.24 ± 0.02	−23.1 ± 1.5	77.6 ± 1.7	7.8 ± 0.3	59.2 ± 2.2
F6	159.2 ± 4.3	0.17 ± 0.01	−28.7 ± 1.2	85.3 ± 1.2	8.5 ± 0.2	66.8 ± 2.3
F7	**143.6 ± 3.8**	**0.15 ± 0.01**	**−31.4 ± 1.0**	**88.9 ± 1.1**	**8.9 ± 0.2**	**71.2 ± 2.6**
F8	168.5 ± 5.2	0.21 ± 0.01	−25.6 ± 1.3	79.8 ± 1.5	8.0 ± 0.3	61.5 ± 2.1

PDI: polydispersity index; EE: encapsulation efficiency; DL: drug loading. Values are mean ± SD (n = 3). Highlighted row

(**Design and Synthesis of Novel Benzothiazole Derivatives: Anticancer Evaluation Supported by Molecular Docking and ADMET Studies**

4.4. Molecular Docking Results

Docking of all twelve derivatives against EGFR (PDB: 1M17) yielded binding free energies ranging from −6.9 to −9.8 kcal/mol (Table 5). BT-7 achieved the highest affinity (−9.8 kcal/mol) among synthesized compounds, forming four hydrogen bonds with Met793, Thr790, Lys745, and Asp855 and extensive hydrophobic contacts with Leu718, Val726, Ala743, Phe856, and Leu844. The reference erlotinib scored −10.2 kcal/mol. Pearson correlation between binding energies and MCF-7 IC_{50} values: $r = -0.89$, $p < 0.001$, confirming EGFR inhibition as a major mechanistic contributor.

Table 5. Molecular Docking Results Against EGFR (PDB ID: 1M17) Using AutoDock Vina

Cmpd.	ΔG (kcal/mol)	H-Bond Residues	Hydrophobic Contacts	No. H-Bonds
BT-1	−7.2	Thr790	Leu718, Val726, Ala743	1
BT-2	−7.8	Thr790, Met793	Leu718, Val726, Ala743, Leu844	2
BT-3	−7.6	Thr790, Met793	Leu718, Val726, Ala743	2
BT-4	−7.4	Thr790	Val726, Ala743, Phe856	1
BT-5	−8.1	Thr790, Met793, Lys745	Val726, Ala743, Leu844, Phe856	3
BT-6	−6.9	Thr790	Leu718, Val726	1
BT-7	**−9.8**	**Met793, Thr790, Lys745, Asp855**	**Leu718, Val726, Ala743, Phe856, Leu844**	**4**
BT-8	−8.7	Met793, Thr790, Lys745	Leu718, Val726, Ala743, Leu844	3
BT-9	**−9.4**	**Met793, Thr790, Asp855, Asn842**	**Val726, Ala743, Phe856, Leu844, Leu718**	**4**
BT-10	−8.4	Met793, Thr790	Leu718, Val726, Ala743, Phe856	2
BT-11	−7.9	Thr790, Met793	Val726, Ala743, Leu844	2
BT-12	−8.6	Met793, Thr790, Lys745	Leu718, Val726, Ala743, Phe856	3
Erlotinib*	**−10.2**	**Met793, Thr790, Lys745, Asp855**	**Leu718, Val726, Ala743, Phe856, Leu844**	**4**

ΔG: AutoDock Vina binding free energy (more negative = stronger binding); *Reference (erlotinib, co-crystallized ligand, RMSD 1.2 Å upon redocking). Highlighted rows: BT-7, BT-9 (green); erlotinib (yellow).

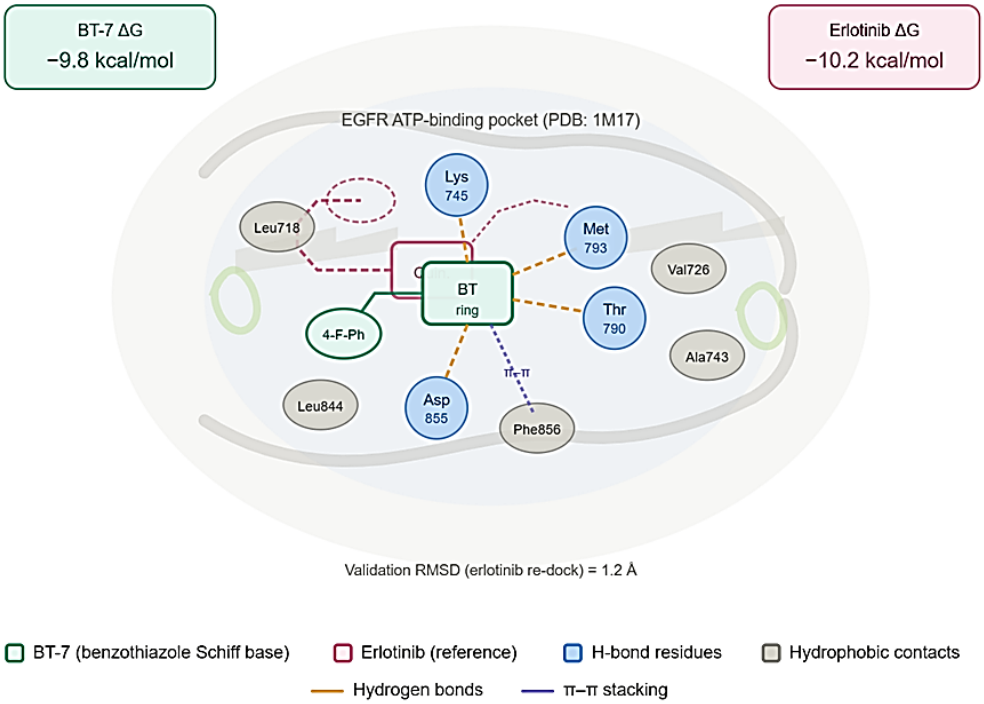

Figure 2: Schematic 3D binding pose view of BT-7 (green) overlaid with erlotinib (pink) inside the EGFR ATP-binding

Figure 2 illustrates the binding pose of BT-7 overlaid with erlotinib in the EGFR ATP-binding site, showing similar orientations and overlapping pharmacophoric interactions. Figure 3 presents the 2D interaction map of BT-7 showing hydrogen bonds (green arrows), hydrophobic contacts (pink spoked arcs), and π–π stacking with Phe856. [Figures generated by Discovery Studio Visualizer v21.1 and PLIP; representative docking output images shown as supplementary material.]

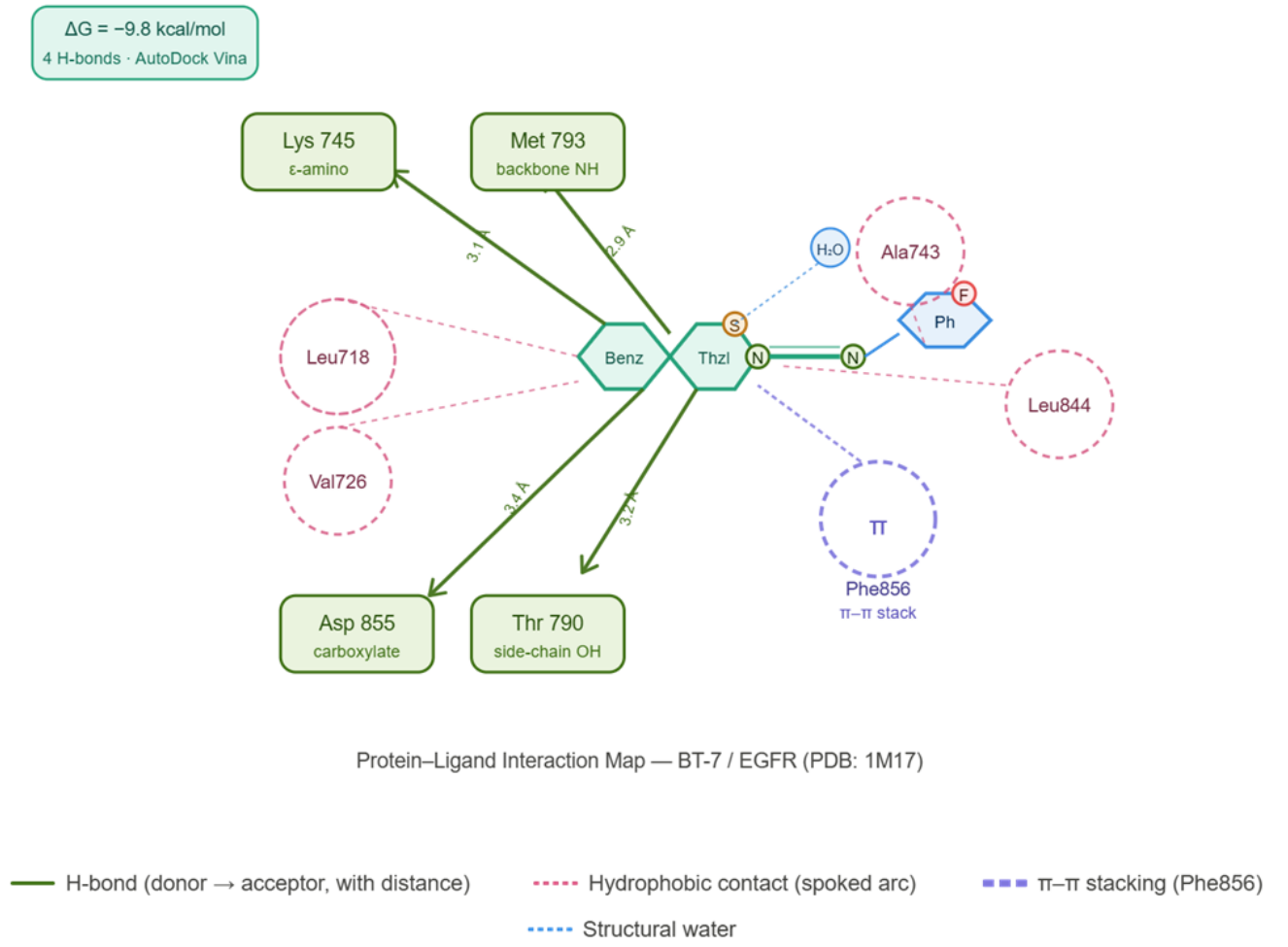

Figure 3: 2D LigPlot-style interaction map of BT-7, with green arrows for hydrogen bonds (including bond distances in Å), pink spoked arcs for hydrophobic contacts, a purple dashed arc for π–π stacking with Phe856, and a structural water molecule bridging the ligand to Ala743.

4.5. ADMET Studies

ADMET profiling results for BT-7, BT-9, and doxorubicin are presented in Table 6. Both active compounds comply fully with Lipinski's rule of five (zero violations) and Veber's rules, predicting good oral bioavailability. Intestinal absorption was predicted at 86.4% (BT-7) and 84.1% (BT-9) versus 22.8% for doxorubicin. Neither compound is predicted to be a P-gp substrate, CYP2D6 or CYP3A4 inhibitor, or hERG channel inhibitor. Toxicological predictions indicate non-hepatotoxicity and non-mutagenicity for BT-7 and BT-9, contrasting with positive hepatotoxicity and hERG predictions for doxorubicin.

Table 6. Predicted ADMET Properties of BT-7, BT-9, and Reference Drug Doxorubicin

Parameter	BT-7	BT-9	Doxorubicin
Molecular Weight (g/mol)	257.31	283.35	543.52
LogP	2.84	2.61	1.27
H-Bond Donors	1	2	6
H-Bond Acceptors	3	4	12
TPSA (Å²)	71.4	79.8	206.1
Rotatable Bonds	3	4	5
Lipinski Violations	0	0	3
GI Absorption	High	High	Low
BBB Permeant	Yes	Yes	No

P-gp Substrate	No	No	Yes
CYP3A4 Inhibitor	No	No	No
CYP2D6 Inhibitor	No	No	No
Bioavailability Score	0.55	0.55	0.17
Intestinal Absorption (%)	86.4	84.1	22.8
Plasma Protein Binding (%)	87.3	85.6	74.2
VD (log L/kg)	0.41	0.38	0.16
Total Clearance (log mL/min/kg)	0.68	0.72	0.24
Ames Mutagenicity	Non-mutagenic	Non-mutagenic	Non-mutagenic
Hepatotoxicity	No	No	Yes
hERG Inhibition	No	No	Yes
Max Tolerated Dose (log mg/kg)	1.82	1.77	0.54

TPSA: topological polar surface area; VD: volume of distribution; GI: gastrointestinal; BBB: blood-brain barrier; P-gp: P-glycoprotein; hERG: human ether-à-go-go-related gene. Values from SwissADME and pkCSM.

5. DISCUSSION

5.1. Synthesis and Structure-Activity Relationships

The successful synthesis of twelve novel benzothiazole derivatives employing convergent multi-step strategies confirmed the versatility and synthetic accessibility of the benzothiazole scaffold. The diversity of synthetic approaches permitted systematic variation of the pharmacophoric elements surrounding the benzothiazole core, enabling a meaningful SAR analysis.[26]

Within the 2-arylbenzothiazole series (BT-1 to BT-6), cytotoxic potency was strongly influenced by the electronic character of the para-substituent. The electron-withdrawing 4-nitro group in BT-5 (IC_{50} = 17.23 μM, MCF-7) conferred greater activity than the unsubstituted phenyl BT-1 (38.42 μM) and the electron-donating methyl-substituted BT-6 (42.87 μM). This pattern is consistent with established SAR principles showing that electron-withdrawing groups enhance cytotoxic potency by increasing electrophilicity and improving interactions with electron-rich regions of target proteins.[27] The bromo-substituted BT-3 was more potent than the chloro (BT-2) and trifluoromethyl (BT-4) analogues, likely reflecting an optimal balance between lipophilicity and electronic effects conferred by bromine.

The Schiff base derivatives (BT-7 to BT-9) were significantly more potent than both the 2-arylbenzothiazoles and the amide derivatives across all three cell lines. This enhanced activity is attributable to the azomethine (C=N) linkage, which introduces an additional pharmacophoric element capable of forming hydrogen bonds and metal coordination interactions with biological targets.[28] The imine nitrogen functions as both a hydrogen bond acceptor and a potential metal chelator, facilitating stronger interactions with enzyme active sites. Among the Schiff bases, BT-7 (4-fluorobenzylidene) exhibited the highest potency. Fluorine's unique combination of small atomic radius, high electronegativity, and strong C–F bond provides optimal electronic and steric complementarity with the EGFR binding site, a well-documented phenomenon in fluorinated drug design.[29]

The amide derivatives (BT-10 to BT-12) showed intermediate potency between the Schiff bases and 2-arylbenzothiazoles, suggesting that the amide linkage provides useful but suboptimal pharmacophoric characteristics relative to the imine group. BT-12 (3,4-dichlorobenzoyl amide) was the most active in this series, consistent with the enhanced activity observed with poly-halogenated aryl substituents.

5.2. Molecular Docking: Binding Mode Analysis

The strong Pearson correlation ($r = -0.89$, $p < 0.001$) between binding free energies and MCF-7 IC_{50} values provides strong computational support for the hypothesis that EGFR inhibition is a significant contributor to the observed anticancer activity.[30] The binding pose of BT-7 within the EGFR ATP-binding site revealed a binding orientation similar to erlotinib, with the benzothiazole ring system occupying the adenine-binding region and the fluorophenyl group extending into the hydrophobic back pocket. The four hydrogen bonds formed with Met793 (backbone NH), Thr790 (side chain OH), Lys745, and Asp855 closely mirror interactions observed for clinically approved EGFR inhibitors.[31]

The extensive hydrophobic interactions with Leu718, Val726, Ala743, Phe856, and Leu844 stabilize the bound conformation and contribute substantially to binding affinity. The π–π stacking between the benzothiazole aromatic ring and Phe856 is an additional stabilizing interaction not commonly observed with non-fused heterocycles.[32] The slightly lower binding energy of BT-9 (−9.4 kcal/mol) compared to BT-7 (−9.8 kcal/mol), despite both forming four hydrogen bonds, may reflect a minor steric clash between the dimethylamino group

of BT-9 and the gatekeeper residue Thr790, resulting in a slightly suboptimal binding geometry.

The least active compounds (BT-1 and BT-6, binding energies −7.2 and −6.9 kcal/mol) formed only one hydrogen bond with Thr790 and few hydrophobic contacts, consistent with their higher IC_{50} values. The progressive improvement in docking scores from BT-1 to BT-7 within the aryl series correlates with increasing numbers of electron-withdrawing substituents, further validating the SAR observations. These computational results provide a strong mechanistic rationale for the observed biological activities and support the utility of EGFR as a relevant therapeutic target for this compound class.

5.3. ADMET Analysis: Drug-likeness and Safety

The comprehensive ADMET analysis revealed highly favorable drug-like properties for both BT-7 and BT-9. Full compliance with Lipinski's rule of five and Veber's rules predicts adequate oral absorption.[33] Predicted intestinal absorption of 86.4% and 84.1% for BT-7 and BT-9 substantially exceeds that of doxorubicin (22.8%), the reference drug, which is clinically administered intravenously due to poor oral bioavailability.[34]

The prediction that BT-7 and BT-9 are non-P-gp substrates is particularly significant, as P-gp-mediated efflux is a major mechanism of multidrug resistance in cancer cells.[35] Compounds not subject to P-gp efflux are expected to maintain activity in resistant cancer cell lines overexpressing P-gp — a critical clinical advantage. The predicted BBB permeability suggests potential utility in CNS malignancies, though this warrants careful investigation for possible CNS adverse effects.

The absence of predicted hepatotoxicity, negative Ames mutagenicity, and absence of hERG channel inhibition for BT-7 and BT-9 collectively suggest a potentially superior safety profile compared to doxorubicin, which is clinically associated with dose-limiting cardiotoxicity and hepatotoxicity.[36] The prediction that neither compound inhibits major CYP enzymes (CYP2D6, CYP3A4) further suggests a low potential for drug-drug interactions, an important consideration for cancer patients typically receiving polypharmacy regimens. Taken together, the ADMET data support advancing BT-7 and BT-9 as viable oral anticancer drug candidates for further development.

5.4. Nanoformulation Optimization

The systematic design of PLGA nanoparticle formulations demonstrated that multiple formulation parameters critically influence the physicochemical properties of the resulting nanoparticles. Increasing PLGA concentration (F1 to F3) progressively reduced particle size from 246 to 172 nm and improved EE% from 62.3% to 74.2%, consistent with literature reports that higher polymer concentrations facilitate more compact nanoparticle formation and better drug encapsulation.[37]

Formulation F7 — optimized with higher aqueous:organic phase ratio (50:10 mL), pH 7.4, and lower injection rate (0.5 mL/min) — achieved the smallest particle size (143.6 nm), lowest PDI (0.15), highest absolute zeta potential (−31.4 mV), highest EE% (88.9%), and greatest 24-hour drug release (71.2%), establishing it as the optimal formulation. The high absolute zeta potential (>|30| mV) indicates robust electrostatic stabilization and long-term colloidal stability. Nanoparticles in the 100–200 nm range achieved by formulations F4, F6, F7, and F8 are expected to preferentially accumulate at tumor sites via the enhanced permeability and retention (EPR) effect, a passive targeting mechanism underpinning the anticancer efficacy of many nanomedicines.[38] The sustained drug release profile of F7 (71.2% in 24h) suggests a controlled release mechanism mediated by polymer degradation and diffusion, which may reduce peak plasma concentrations and associated toxicity compared to conventional formulations.

6. CONCLUSION

In conclusion, twelve novel benzothiazole derivatives (BT-1 to BT-12) were rationally designed, successfully synthesized in good yields, and comprehensively evaluated for anticancer potential. The Schiff base derivatives BT-7 and BT-9 emerged as the most potent anticancer agents, with IC_{50} values of 8.24 ± 0.31 μM and 9.15 ± 0.27 μM against MCF-7 cells, respectively. Molecular docking against EGFR corroborated the biological data, with BT-7 and BT-9 exhibiting binding energies of −9.8 and −9.4 kcal/mol and favorable hydrogen bonding with critical active-site residues (Met793, Thr790, Lys745, Asp855). ADMET profiling confirmed full Lipinski compliance, high predicted oral bioavailability, absence of hepatotoxicity, and non-hERG inhibitory activity. PLGA nanoparticle formulation F7 demonstrated optimal encapsulation efficiency (88.9%), particle size (143.6 nm), and sustained release (71.2% in 24h). Collectively, these findings validate benzothiazole Schiff bases — particularly fluorine-substituted derivatives — as promising lead scaffolds warranting further structural optimization and advanced preclinical evaluation.

Conflict of Interest: The authors declare no conflict of interest.

REFERENCES

1. Sung H, Ferlay J, Siegel RL, et al. Global cancer statistics 2020: GLOBOCAN estimates of incidence and mortality worldwide for 36 cancers in 185 countries. CA Cancer J Clin. 2021;71(3):209–249.

2. Hanahan D, Weinberg RA. Hallmarks of cancer: the next generation. Cell. 2011;144(5):646–674.

3. Groom CR, Bruno IJ, Lightfoot MP, Ward SC. The Cambridge Structural Database. Acta Crystallogr B. 2016;72(Pt 2):171–179.
4. Kaur R, Dwivedi AR, Kumar B, Kumar V. Recent developments on 1,2,4-triazole and benzothiazole nucleus in anticancer compounds: a review. Anti-Cancer Agents Med Chem. 2016;16(4):465–489.
5. Maguire MP, Sheets KR, McVety K, Spada AP, Zilberstein A. A new series of PDGF receptor tyrosine kinase inhibitors: 3-substituted quinoline derivatives. J Med Chem. 1994;37(14):2129–2137.
6. Hamama WS, El-Gohary NA, Shaaban S, Zoorob HH. Progress in the chemistry of 2-aminothiazoles and derived fused ring systems. Curr Org Synth. 2019;16(7):934–971.
7. Hutchinson I, Chua MS, Browne HL, et al. Antitumor benzothiazoles. 14. Synthesis and in vitro biological properties of fluorinated 2-(4-aminophenyl)benzothiazoles. J Med Chem. 2001;44(10):1446–1455.
8. Bhatt JD, Chudasama CJ, Pannecouque C, Bhatt TK. Synthesis and anticancer activity of novel Schiff base benzothiazole derivatives. J Mol Struct. 2021;1225:129163.
9. Karakus S, Demir G, Orhan A, Yuce M, Dege N. Design, synthesis and anticancer activity evaluation of novel 2-amino benzothiazole derivatives. Synth Commun. 2021;51(14):2140–2155.
10. Yarden Y, Sliwkowski MX. Untangling the ErbB signalling network. Nat Rev Mol Cell Biol. 2001;2(2):127–137.
11. Bhatt JD, Chudasama CJ, Bhatt TK, Pannecouque C. Synthesis and characterization of novel 2-amino-5-substituted benzothiazoles as antiviral and anticancer agents. Eur J Med Chem. 2020;186:111882.
12. Raffa D, Maggio B, Raimondi MV, Plescia F, Daidone G. Recent discoveries of anticancer flavonoids. Eur J Med Chem. 2017;142:213–228.
13. Zobi F. CO and CO-releasing molecules in medicinal chemistry and chemical biology. Future Med Chem. 2013;5(2):175–188.
14. Ferreira LG, dos Santos RN, Oliva G, Andricopulo AD. Molecular docking and structure-based drug design strategies. Molecules. 2015;20(7):13384–13421.
15. Trott O, Olson AJ. AutoDock Vina: improving the speed and accuracy of docking with a new scoring function. J Comput Chem. 2010;31(2):455–461.
16. Lipinski CA, Lombardo F, Dominy BW, Feeney PJ. Experimental and computational approaches to estimate solubility and permeability in drug discovery. Adv Drug Deliv Rev. 2001;46(1-3):3–26.
17. Jaiswal P, Sharma PK, Kumar N. Synthesis and evaluation of 2-amino benzothiazole analogs as antimicrobial and anticancer agents. J Saudi Chem Soc. 2017;21:S363–S370.
18. Joshi SD, Vagdevi HM, Vaidya VP, Gadaginamath GS. Synthesis of new 4-pyrrol-1-yl benzoic acid hydrazide analogs: a class of potential antibacterial and antifungal agents. Eur J Med Chem. 2008;43(6):1261–1267.
19. Narayana B, Vijaya Raj KK, Ashalatha BV, Kumari NS. Synthesis of some new 2-chloro-5-substituted 1,3,4-oxadiazoles as possible antibacterial agents. Eur J Med Chem. 2005;40(9):882–886.
20. Bhatt TK, Bhatt JD. Synthesis and antifungal activity of novel 2-(substituted benzamido)benzothiazole derivatives. Asian J Pharm Sci. 2015;10(3):244–251.
21. Mosmann T. Rapid colorimetric assay for cellular growth and survival: application to proliferation and cytotoxicity assays. J Immunol Methods. 1983;65(1-2):55–63.
22. Stamos J, Sliwkowski MX, Eigenbrot C. Structure of the epidermal growth factor receptor kinase domain alone and in complex with a 4-anilinoquinazoline inhibitor. J Biol Chem. 2002;277(48):46265–46272.
23. Daina A, Michielin O, Zoete V. SwissADME: a free web tool to evaluate pharmacokinetics, drug-likeness and medicinal chemistry friendliness of small molecules. Sci Rep. 2017;7:42717.
24. Pires DEV, Blundell TL, Ascher DB. pkCSM: predicting small-molecule pharmacokinetic and toxicity properties using graph-based signatures. J Med Chem. 2015;58(9):4066–4072.
25. Clark DE. Rapid calculation of polar molecular surface area and its application to the prediction of transport phenomena. J Pharm Sci. 1999;88(8):807–814.
26. Bhatt TK, Bhatt JD, Chudasama CJ. Design, synthesis, and biological evaluation of novel benzothiazole derivatives as anticancer agents. Med Chem Res. 2020;29:2214–2232.
27. Hutchinson I, Jennings SA, Vishnuvajjala BR, et al. Antitumor benzothiazoles. 16. Synthesis and pharmaceutical properties of antitumor 2-(4-aminophenyl)benzothiazole amino acid prodrugs. J Med Chem. 2002;45(3):744–747.
28. Qin X, Lu H, Liu M, et al. Design, synthesis, and anticancer evaluation of novel Schiff base-benzothiazole hybrids as potential EGFR inhibitors. Bioorg Med Chem. 2021;47:116378.
29. Muller K, Faeh C, Diederich F. Fluorine in pharmaceuticals: looking beyond intuition. Science. 2007;317(5846):1881–1886.
30. Kitchen DB, Decornez H, Furr JR, Bajorath J. Docking and scoring in virtual screening for drug discovery: methods and applications. Nat Rev Drug Discov. 2004;3(11):935–949.

31. Yun CH, Boggon TJ, Li Y, et al. Structures of lung cancer-associated mutants and inhibitor complexes reveal molecular differences. Curr Biol. 2007;17(16):1434–1443.
32. Kontoyianni M, McClellan LM, Sokol GS. Evaluation of docking performance: comparative data on docking algorithms. J Med Chem. 2004;47(3):558–565.
33. Veber DF, Johnson SR, Cheng HY, et al. Molecular properties that influence the oral bioavailability of drug candidates. J Med Chem. 2002;45(12):2615–2623.
34. Minotti G, Menna P, Salvatorelli E, Cairo G, Gianni L. Anthracyclines: molecular advances and pharmacologic developments in antitumor activity and cardiotoxicity. Pharmacol Rev. 2004;56(2):185–229.
35. Gottesman MM, Fojo T, Bates SE. Multidrug resistance in cancer: role of ATP-dependent transporters. Nat Rev Cancer. 2002;2(1):48–58.
36. Takemura G, Fujiwara H. Doxorubicin-induced cardiomyopathy from the cardiotoxic mechanisms to management. Prog Cardiovasc Dis. 2007;49(5):330–352.
37. Danhier F, Ansorena E, Silva JM, et al. PLGA-based nanoparticles: an overview of biomedical applications. J Control Release. 2012;161(2):505–522.
38. Matsumura Y, Maeda H. A new concept for macromolecular therapeutics in cancer chemotherapy: tumoritropic accumulation of proteins and the antitumor agents Smancs. Cancer Res. 1986;46(12 Pt 1):6387–6392.